The Journal of Chemical Physics

Active chiral molecules in activity gradients

Cite as: J. Chem. Phys. **157**, 134902 (2022); https://doi.org/10.1063/5.0109817
Submitted: 14 July 2022 • Accepted: 09 September 2022 • Accepted Manuscript Online: 12 September 2022 • Published Online: 07 October 2022

Pietro Luigi Muzzeddu, Hidde Derk Vuijk, Hartmut Löwen, et al.

View Online Export Citation CrossMark

ARTICLES YOU MAY BE INTERESTED IN

Path integral description of semiflexible active Brownian polymers
The Journal of Chemical Physics **156**, 064105 (2022); https://doi.org/10.1063/5.0081020

Analytical approach to chiral active systems: Suppressed phase separation of interacting Brownian circle swimmers
The Journal of Chemical Physics **156**, 194904 (2022); https://doi.org/10.1063/5.0085122

Vibrational Levels of a Generalized Morse Potential
The Journal of Chemical Physics (2022); https://doi.org/10.1063/5.0103433

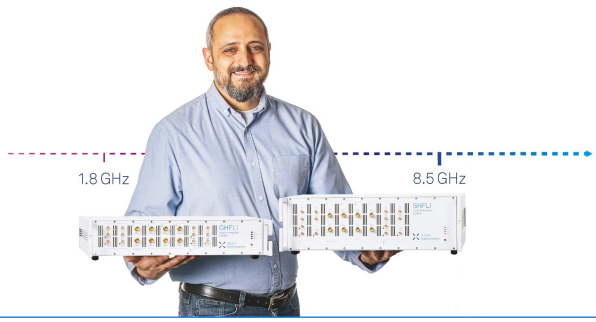

Trailblazers. New
Meet the Lock-in Amplifiers that measure microwaves.
Zurich Instruments
Find out more

© 2022 Author(s).

The Journal of Chemical Physics ARTICLE scitation.org/journal/jcp

Active chiral molecules in activity gradients

Cite as: J. Chem. Phys. 157, 134902 (2022); doi: 10.1063/5.0109817
Submitted: 14 July 2022 • Accepted: 9 September 2022 •
Published Online: 7 October 2022

View Online Export Citation CrossMark

Pietro Luigi Muzzeddu,[1,a)] Hidde Derk Vuijk,[2] Hartmut Löwen,[3] Jens-Uwe Sommer,[2,4] and Abhinav Sharma[2,4]

AFFILIATIONS

[1] SISSA–International School for Advanced Studies, I-34136 Trieste, Italy
[2] Leibniz-Institut für Polymerforschung Dresden, Institut Theory der Polymere, 01069 Dresden, Germany
[3] Institut für Theoretische Physik II: Weiche Materie, Heinrich-Heine-Universität Düsseldorf, 40225 Düsseldorf, Germany
[4] Technische Universität Dresden, Institut für Theoretische Physik, 01069 Dresden, Germany

[a)] **Author to whom correspondence should be addressed:** pmuzzedd@sissa.it

ABSTRACT

While the behavior of active colloidal molecules is well studied now for constant activity, the effect of activity gradients is much less understood. Here, we explore one of the simplest molecules in activity gradients, namely active chiral dimers composed of two particles with opposite active torques of the same magnitude. We show analytically that with increasing torque, the dimer switches its behavior from antichemotactic to chemotactic. The origin of the emergent chemotaxis is the cooperative exploration of an activity gradient by the two particles. While one of the particles moves into higher activity regions, the other moves towards lower activity regions, resulting in a net bias in the direction of higher activity. We do a comparative study of chiral active particles with charged Brownian particles under a magnetic field and show that despite the fundamental similarity in terms of their odd-diffusive behavior, their dynamics and chemotactic behavior are generally not equivalent. We demonstrate this explicitly in a dimer composed of oppositely charged active particles, which remains antichemotactic to any magnetic field.

Published under an exclusive license by AIP Publishing. https://doi.org/10.1063/5.0109817

I. INTRODUCTION

Living matter at the micron scale is able to perform a wide variety of complex motions and behaviors; see e.g., Refs. 1 and 2. This requires sensing chemical and structural properties of the environment, processing this information by complex biochemical networks, and adapting behavior accordingly.[3–5] For example, the bacterium *E. coli* measures the local nutrient concentration while it swims and compares that with the concentration in the past. If the current concentration is getting lower (higher), it increases (decreases) its tumble rate. This strategy results in chemotaxis, i.e., preferential accumulation in regions where the nutrient concentration is high.[6,7]

Active particles are regarded as the simplest models for motility in living systems. While they share the essential features, namely self-propulsion and persistence, with the bacteria, their response to local fuel concentration is rather simple; they merely adjust the speed in proportion to the local fuel concentration,[8–12] a mechanism known as orthokinesis.[13] As a consequence, active particles subjected to fuel gradients preferentially accumulate in regions where the fuel concentration is low.[14,15] Nevertheless, the ability to steer active particles towards the correct target zone—artificial chemotaxis—remains a highly sought property of synthetic active matter. While this has been demonstrated experimentally via elaborate feedback mechanisms,[16–18] where an external stimulus is applied to the particle as a function of its state (position and orientation), the continuous monitoring of the particle's state might not always be possible. Therefore, an autonomous approach where some form of feedback emerges spontaneously is much more desirable and can correctly steer the active particle towards the target without requiring external stimuli.

Recently, we showed that chemotaxis can emerge in a system of cargo carrying active particles.[19] While active particles with light cargo accumulate in regions of low activity, a crossover occurs with increasing cargo such that the active-passive complex accumulates in regions of high activity. For a heavy cargo, which moves much more slowly than the active particle, the active particle *performs* a local integration of the activity profile in the neighborhood of the attached cargo, resulting in a net force towards the regions of higher activity, giving rise to chemotactic behavior. Active particles

Published under an exclusive license by AIP Publishing

connected in a chain to form polymers have recently received much attention.[20–25] We showed that active polymers are qualitatively similar to a single active particle coupled to a passive cargo.[19] While short chains are antichemotactic, chains with four or more particles exhibit chemotactic behavior.

In this paper, we extend the idea of emergent chemotaxis to colloidal molecules made of active chiral particles (ACPs). Specifically, we consider a dimer composed of two active chiral particles driven by opposite torques in an activity gradient (see schematic in Fig. 1). With increasing torque, the active chiral dimer switches its behavior from antichemotactic to chemotactic and accumulates in regions of high activity. Unlike a single active particle, which only performs chemokinesis,[13] the preferential accumulation of the dimer in the high or low activity regions can be regarded as genuine chemotaxis. While the behavior of active colloidal molecules is well understood for constant activity,[26,27] the effect of activity gradients is much less explored. Very recently, we studied how a rigid dimer composed of two active particles with orientations fixed with respect to the connecting bond behaves in activity gradients.[28] In contrast, in an active chiral dimer, the orientations of the two particles evolve freely due to the thermal and chiral torques.

Active chiral particles exhibit odd-diffusive motion on time scales greater than the persistence time.[29] The diffusion tensor that characterizes the overdamped motion contains both a symmetric and an antisymmetric part. Both passive and self-propelled charged Brownian particles also perform odd-diffusive motion under the effect of the Lorentz force.[30–34] While active chiral particles rotate due to the microscopic active torque, in the case of charged particles under a magnetic field, a certain handedness is introduced by the Lorentz force. At a coarse-grained level, where one integrates out the orientational degree of freedom, the two systems present many similarities. One can even map the two model systems for homogeneous magnetic fields, activity, and torque. However, as expected, the mapping does not hold in general. We show this explicitly by analyzing their chemotactic behavior: a dimer composed of oppositely charged active particles always accumulates in the regions of low activity independently of the applied magnetic field.

This paper is organized as follows: In Sec. II, we present our model of a dimer composed of two active chiral particles driven by opposite torques of the same magnitude. We derive a coarse-grained Fokker–Planck equation from which we obtain an analytical prediction for the density distribution of the dimer. In Sec. III, inspired by the similarity between an ACP and a charged self-propelled particle subjected to Lorentz force in terms of their odd diffusive behavior, we construct a dimer of these active charged particles and show that, unlike a dimer of ACPs with opposite torques, there is no magnetic field governed crossover in the tactic behavior. Finally, in Sec. IV, we discuss possible experimental realizations and present a brief outlook for future work.

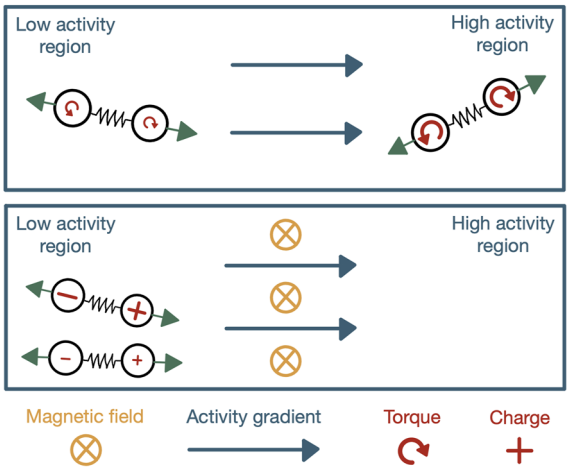

FIG. 1. Dimers in activity gradients. In the upper panel, both particles experience homogeneous torques in the direction perpendicular to the plane of motion, giving rise to their chiral motion (curved arrows). When the active torque is small, the dimer accumulates in the region of low activity (antichemotactic). Beyond a threshold of active torque, the dimer switches its tactic behavior, i.e., it accumulates in the region of high activity. The lower panel shows a dimer composed of oppositely charged particles. While the particles experience an active force, there is no active torque acting on them. Instead, the dimer is subjected to a homogeneous external magnetic field. The charged active dimer always shows antichemotactic behavior, i.e., unlike its torque-driven counterpart, there is no magnetic field governed crossover in its tactic behavior.

II. DIMER OF ACTIVE CHIRAL PARTICLES

We consider a two-dimensional system of a dimer composed of two active chiral particles interacting via an attractive potential $U(\boldsymbol{r})$ (e.g., a spring or a rigid rod). In addition to (thermal) rotational diffusion, both particles experience homogeneous torques in the direction perpendicular to the plane of motion, giving rise to their chiral motion. We restrict our analysis to opposite torques $(\omega, -\omega)$ on the two active particles. The overdamped dynamics of the system is governed by the following Langevin equations:[35]

$$\begin{aligned}
\frac{d\boldsymbol{r}_1}{dt} &= -\frac{1}{\gamma}\nabla_1 U(\boldsymbol{r}_1-\boldsymbol{r}_2) + v_a(\boldsymbol{r}_1)\boldsymbol{p}_1 + \sqrt{2D_T}\boldsymbol{\xi}_1(t),\\
\frac{d\boldsymbol{r}_2}{dt} &= +\frac{1}{\gamma}\nabla_1 U(\boldsymbol{r}_1-\boldsymbol{r}_2) + v_a(\boldsymbol{r}_2)\boldsymbol{p}_2 + \sqrt{2D_T}\boldsymbol{\xi}_2(t),\\
\frac{d\theta_1}{dt} &= +\omega + \sqrt{2D_R}\eta_1(t),\\
\frac{d\theta_2}{dt} &= -\omega + \sqrt{2D_R}\eta_2(t),
\end{aligned} \tag{1}$$

where $\boldsymbol{p}_i = (\cos(\theta_i),\ \sin(\theta_i))$ are the orientation vectors and $\boldsymbol{\xi}_1(t), \boldsymbol{\xi}_2(t), \eta_1(t), \eta_2(t)$ are independent random Gaussian vectors with the following statistical properties:

$$\begin{aligned}
\langle\boldsymbol{\xi}_1(t)\rangle &= \langle\boldsymbol{\xi}_2(t)\rangle = \langle\boldsymbol{\eta}(t)\rangle = 0,\\
\langle\boldsymbol{\xi}_1(t)\boldsymbol{\xi}_1^T(s)\rangle &= \langle\boldsymbol{\xi}_2(t)\boldsymbol{\xi}_2^T(s)\rangle = \mathbf{1}\delta(t-s),\\
\langle\eta_1(t)\eta_1(s)\rangle &= \langle\eta_2(t)\eta_2(s)\rangle = \delta(t-s).
\end{aligned} \tag{2}$$

The two ACPs composing the dimer have the same friction coefficient γ, translational diffusion coefficient $D_T = \frac{k_B T}{\gamma}$ and rotational diffusion coefficient D_R. In our model, the rotational

Published under an exclusive license by AIP Publishing

diffusion coefficient is a free parameter.[36–38] The two ACPs are self-propelled along the direction given by their orientation vectors $(\boldsymbol{p}_1, \boldsymbol{p}_2)$ with an intensity set by the activity function $v_a(\boldsymbol{r})$, which we assume being positively correlated with a local fuel concentration. The additional torque acting on each particle produces a systematic rotation of the orientation vector around the fixed z-axis. Note that we do not take into account the torque on the two active particles due to the activity gradient because this depends on the specific self-propulsion mechanism.[39,40] However, this torque can be included in the analysis presented here. We also ignore the hydrodynamic interaction between the two particles and their effect on self-propulsion.[41–44]

The relative importance of the deterministic and stochastic contributions to the $\boldsymbol{p}_i$ (or θ_i) dynamics plays a crucial role in determining the behavior of our system, as shown in the following. Since we are interested in where dimers accumulate at steady state, we aim to find an expression for the coarse-grained density as a function of the dimer's center of mass only. After rewriting the dynamics in terms of the collective coordinate $\boldsymbol{R} = \frac{\boldsymbol{r}_1+\boldsymbol{r}_2}{2}$ and the inner coordinate $\boldsymbol{r} = \boldsymbol{r}_1 - \boldsymbol{r}_2$, the related Fokker–Planck equation reads as

$$\begin{aligned}\partial_t P(\boldsymbol{R},\boldsymbol{r},\theta_1,\theta_2,t) = &-\nabla_{\boldsymbol{R}}\cdot\left[\frac{1}{2}v_a\left(\boldsymbol{R}+\frac{\boldsymbol{r}}{2}\right)\boldsymbol{p}_1 P\right] - \nabla_{\boldsymbol{R}}\cdot\left[\frac{1}{2}v_a\left(\boldsymbol{R}-\frac{\boldsymbol{r}}{2}\right)\boldsymbol{p}_2 P - \frac{D_T}{2}\nabla_{\boldsymbol{R}} P\right] - \nabla_{\boldsymbol{r}}\cdot\left[\frac{2}{\gamma}\boldsymbol{F}P\right]\\ &- \nabla_{\boldsymbol{r}}\cdot\left[v_a\left(\boldsymbol{R}+\frac{\boldsymbol{r}}{2}\right)\boldsymbol{p}_1 P - v_a\left(\boldsymbol{R}-\frac{\boldsymbol{r}}{2}\right)\boldsymbol{p}_2 P - 2D_T\nabla_{\boldsymbol{r}} P\right] - \frac{\partial}{\partial\theta_1}\left[\omega P - D_R\frac{\partial P}{\partial\theta_1}\right] - \frac{\partial}{\partial\theta_2}\left[-\omega P - D_R\frac{\partial P}{\partial\theta_2}\right].\end{aligned} \tag{3}$$

One can now proceed by expanding the joint probability distribution $P(\boldsymbol{R},\boldsymbol{r},\theta_1,\theta_2,t)$ into the eigenfunctions of the operator $\hat{\mathcal{R}}^2 = \frac{\partial^2}{\partial\theta_1^2} + \frac{\partial^2}{\partial\theta_2^2}$. This angular multipole expansion leads to the following expression:

$$\begin{aligned}P(\boldsymbol{R},\boldsymbol{r},\theta_1,\theta_2,t) = \frac{1}{\Omega_2^2}\Big[&\phi + \boldsymbol{\sigma}_1\cdot\boldsymbol{p}_1 + \boldsymbol{\sigma}_2\cdot\boldsymbol{p}_2 + \underline{\underline{\boldsymbol{\sigma}}}_{1,2} : \boldsymbol{p}_1\boldsymbol{p}_2\\ &+ \underline{\underline{\boldsymbol{w}}}_1 : \left(\boldsymbol{p}_1\boldsymbol{p}_1 - \frac{\mathbf{1}}{2}\right) + \underline{\underline{\boldsymbol{w}}}_2 : \left(\boldsymbol{p}_2\boldsymbol{p}_2 - \frac{\mathbf{1}}{2}\right) + \cdots\Big].\end{aligned} \tag{4}$$

A hierarchy of equations for the coefficients $(\phi, \boldsymbol{\sigma}_1, \boldsymbol{\sigma}_2, \underline{\underline{\boldsymbol{\sigma}}}_{1,2}, \underline{\underline{\boldsymbol{w}}}_1, \underline{\underline{\boldsymbol{w}}}_2, \ldots)$ can be obtained by projecting the FPE onto their relative eigenfunctions. We focus on the case where the activity function is slowly varying in space. This small gradient assumption allows us to decouple the equations for the various coefficients in the hierarchy and to find an effective equation for the coarse grained density,

$$\rho(\boldsymbol{R}) = \int d\boldsymbol{r}\,\phi(\boldsymbol{R},\boldsymbol{r}). \tag{5}$$

Details of the coarse graining procedure and the calculation of the steady-state properties are shown in the supplementary material, Sec. S1.

In particular, when the attractive interaction corresponds to a spring with zero rest length, i.e., $U(\boldsymbol{r}) = \frac{k}{2}\boldsymbol{r}^2$, the coarse grained density, $\rho(\boldsymbol{R})$, satisfies the following Fokker–Planck equation:

$$\begin{aligned}\partial_t\rho(\boldsymbol{R}) &= -\nabla_{\boldsymbol{R}}\cdot[\boldsymbol{V}(\boldsymbol{R})\rho(\boldsymbol{R}) - D(\boldsymbol{R})\nabla_{\boldsymbol{R}}\rho(\boldsymbol{R})],\\ D(\boldsymbol{R}) &= \frac{1}{1+\Omega^2}\frac{v_a^2(\boldsymbol{R})}{4D_R} + \frac{D_T}{2},\\ \boldsymbol{V}(\boldsymbol{R}) &= -\frac{1}{2}\epsilon\nabla_{\boldsymbol{R}}D(\boldsymbol{R}),\end{aligned} \tag{6}$$

where $\Omega = \omega/D_R$. The parameter ϵ is defined in terms of dimensionless parameters $\tau = \gamma D_R/2k$ and Ω as

$$\epsilon = \frac{\left(1+(1-\Omega^2)\tau\right)\left(1+\Omega^2\right)}{\left(1+(1-\Omega^2)\tau\right)^2 + \left(\Omega(1+2\tau)\right)^2}. \tag{7}$$

Ω and τ express the active torque and the relaxation time of the spring in units of the rotational diffusion time scale, D_R^{-1}. Since the drift and diffusion terms are related by a derivative relation, it is possible to find an expression for the steady state density without specifying the form of the activity landscape. By imposing a zero flux condition along the direction in which activity varies, one obtains the density

$$\rho(\mathbf{R}) \propto \left[1 + \frac{1}{D_T}\frac{1}{1+\Omega^2}\frac{v_a^2(\mathbf{R})}{2D_R}\right]^{-\frac{1}{2}\epsilon}. \tag{8}$$

In the absence of activity $(v_a(\boldsymbol{R}) = 0)$ the system reduces to a dimer of passive Brownian particles, so we expect a standard diffusive process and a flat distribution at steady state. Notice that if $v_a(\boldsymbol{R}) = 0$, translational and rotational degrees of freedom are decoupled, and the particle's orientation vector does not play any role in the dynamics. In the case of spatially homogeneous activity, the symmetry of the system imposes a flat steady-state distribution again. Indeed, the spatial dependence of $\rho(\boldsymbol{R})$ in (8) is a consequence of the broken spatial invariance due to the inhomogeneous activity landscape.

For a generic spatially varying $v_a(\boldsymbol{R})$, the way activity affects the steady state density profile depends on the sign of ϵ, which in turn is determined by the relative importance of the following two terms: $1+\tau$ and $\Omega^2\tau$. For a fixed spring relaxation time, the competition between rotational diffusion and deterministic active rotation of $\boldsymbol{p}_i$ can lead to qualitatively different scenarios. In particular, if $1+\tau > \Omega^2\tau$, the exponent ϵ is positive and the density peaks in regions of lower activity. In the limiting case of a vanishing active torque, the exponent $\epsilon \to 1/(1+\tau)$. Since the

Published under an exclusive license by AIP Publishing

activity profile reflects the local fuel concentration, we refer to this behavior as antichemotaxis. On the contrary, if $1+\tau < \Omega^2\tau$ dimers accumulate in high activity regions. In the limit of $\omega \to \infty$, the exponent $\epsilon \to -1/\tau$. We call this phenomenon chemotaxis. The crossover between these two regimes occurs at the critical value,

$$\Omega_c = \frac{\omega_c}{D_R} = \sqrt{\frac{1+\tau}{\tau}}, \tag{9}$$

at which the steady state is characterized by a homogeneous density distribution. Figure 2 shows the stationary density distribution of dimers for three different values of ω obtained from simulations of Eq. (1). The theoretical predictions of Eq. (8) are in excellent agreement with the simulations.

At this stage, the following question arises: what is the mechanism responsible for the emergence of a chemotactic phase and why does it require torque values above a certain threshold? To start addressing this point, we focus on the limiting case where the time scale of rotational diffusion is much larger than the spring relaxation time scale, i.e., $\tau \ll 1$ and that of the active torque, i.e., $\Omega \gg 1$. We qualitatively describe the emergence of the chemotactic phase predicted by the model in this regime ($1+\tau \ll \Omega^2\tau$) with the help of a schematic representation of the dynamics shown in Fig. 3. Let us consider a configuration of the dimer in which one of the particles' orientation is in the direction of increasing activity, whereas that of the other is in the direction of decreasing activity. In this configuration, the dimer is typically stretched and experiences a translation towards the higher activity region. Accordingly, the dimer climbs up the activity gradient and the distance between the two particles increases. As the dimer climbs up, the orientations of the two particles evolve due to the active torque such that after some time ($\sim 1/2\omega$) they point towards each other. In this configuration, the dimer experiences a drift towards the low activity region. The dimer thus climbs down the activity gradient; however, while the dimer descends the activity gradient, the two particles approach each other such that the net downward drift continuously decreases before the two particles again point outward as in the initial configuration. Overall, while climbing up, the dimer experiences larger translation due to the two particles getting farther from each other than during the climb down, when the two particles approach each other. In a cycle of period $1/\omega$, the dimer performs a forward and backward motion, with net drift towards the region of higher activities. We based our reasoning on a particular initial configuration. In general, if the rotational diffusion is negligible with respect to the deterministic torque, the mechanism will be somewhat different depending on the initial configuration, but in no case will it bias the motion toward regions of lower activity. Note that for biased movement up to the activity gradient, only a sufficiently large active torque is necessary. The underlying mechanism does not require temporal integration of the fuel concentration,[7] memory,[45] or an explicit coupling between the orientation of the particles and the activity gradients.[40,46,47]

The mechanism presented here relies on the changing distance between the two active particles. In the case of a rigid dimer where the distance between the two particles is fixed, there is no biased movement towards higher activity regions. We show analytically in Sec. S1 of the supplementary material that for a

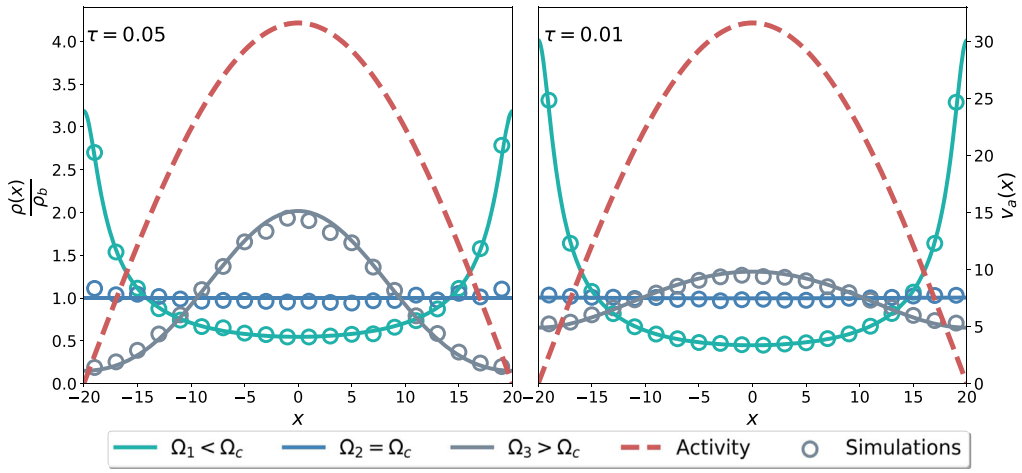

FIG. 2. Steady state density of dimers made by active chiral particles with opposite torque. All lengths and times are measured in units of $l = \sqrt{D_T/D_R}$ and $\tau_r = 1/D_R$, respectively. The numerical density estimation has been carried out by computing the histograms of the time series coming from simulations of the equations of motion (simulation details can be found in Sec. S5 of the supplementary material). Both analytical (continuous line) and numerical (symbols) results have been obtained by adopting periodic boundary conditions. The dashed red curve represents the activity profile, which in this case is homogeneous along y-direction and varying according to $v_a(x) = 10\sqrt{10}\sin(\frac{\pi}{2L}x + \frac{\pi}{2})$ (in units of $\sqrt{D_T D_R}$) along the x-direction, with $2L$ the elementary cell size. Since the system is invariant to translations along the y-direction, we report here the marginal distribution $\rho(x)$ divided by the bulk density. The two figures are characterized by different spring relaxation time scales τ. In particular, for higher stiffness, the density peak in the chemotactic regime is broader and the dimer is less localized. Simulations have been carried out with the following parameters: $\Omega_1 = 2 < \Omega_c$, $\Omega_2 = 4.58257 \approx \Omega_c$, $\Omega_3 = 10 > \Omega_c$, $\tau = 0.05$ on the left panel, and $\Omega_1 = 2 < \Omega_c$, $\Omega_2 = 10.05 \approx \Omega_c$, $\Omega_3 = 15 > \Omega_c$, $\tau = 0.01$ on the right panel.

Published under an exclusive license by AIP Publishing

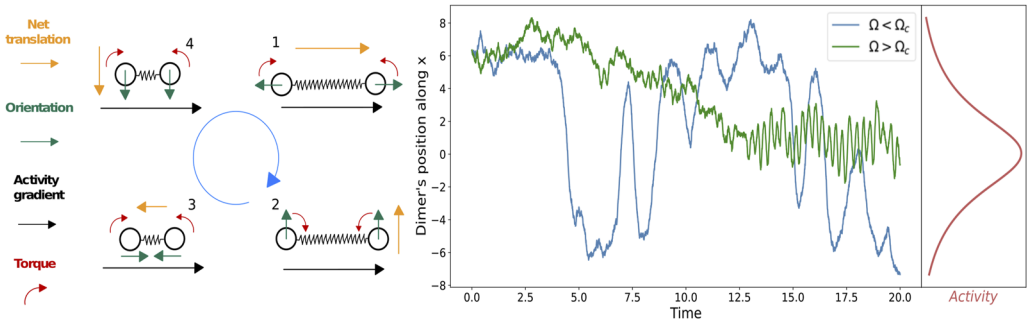

FIG. 3. Left: schematic representation of the mechanism leading to chemotaxis in the case of a dimer made by two active chiral particles with opposite and homogeneous torque (red arrows). The cycle refers to the limiting case of a large time scale related to rotational diffusion compared to the ones of the active torque and spring relaxation, i.e., $\tau \ll 1$ and $\Omega \gg 1$. The orientation vectors (green arrows) are typically opposite when the dimer is stretched (step 1). For this reason, the dimer experiences a translation (orange arrows) in the direction of the activity gradient (black arrows). The evolution of the orientation vectors due to the active torque leads, after some time $\sim 1/2\omega$, to the configuration in step 3, where the system translates towards the low activity region. However, since the spring in step 3 is typically less extended than in 1, this downward drift is much smaller than the one experienced by the dimer in step 1. Overall, this asymmetry results in a biased motion toward high activity regions. For a more detailed representation of the mechanism, see the supplementary material, Video 1. Right: stochastic trajectories obtained from simulations of the equations of motion. Again, all lengths and times are measured in units of $l = \sqrt{D_T/D_R}$ and $\tau_r = 1/D_R$, respectively. In contrast to the blue trajectory $(\Omega = 3 < \Omega_c \simeq 4.58257)$, where the stochasticity due to rotational diffusion prevails on the deterministic rotation induced by the active torque, the green one $(\Omega = 20 > \Omega_c \simeq 4.58257)$ exhibits a directed motion of the dimer's center toward the region where the activity profile (red curve) is higher. This behavior can be regarded as genuine chemotaxis.

rigid dimer $\epsilon = 1/2$. Thus, a rigid active chiral dimer always accumulates in the low activity regions. This is in contrast to the active-passive rigid dimers,[19] where rigid dimers can also exhibit chemotaxis.

Equation (9) defines the critical curve in the (Ω, τ) plane separating the chemotactic phase from the anti-chemotactic one (see Fig. 4). It is interesting to consider the limit $\tau \to 0$, in which case the critical torque scales as $\omega_c \sim \sqrt{kD_R}$. For a fixed D_R, the critical torque diverges in the limit of $k \to \infty$ implying that the dimer preferentially accumulates in the low activity regions. This is indeed expected as, in this case, the two particles are tightly bound to each other, and therefore, the dimer is effectively reduced to a single active particle, which shows antichemotactic behavior. Similarly, for a fixed k, it is apparent that with increasing D_R, one requires an increasingly large active torque to induce chemotactic behavior.

It is important to note that the collective coordinate, $\boldsymbol{R}$, can describe the location of the dimer only when the two particles stay sufficiently close to each other. For small k, the activity gradients can become large on the length scale of the distance between the two particles. Our theory, based on the small-gradient approximation, cannot describe such a situation.

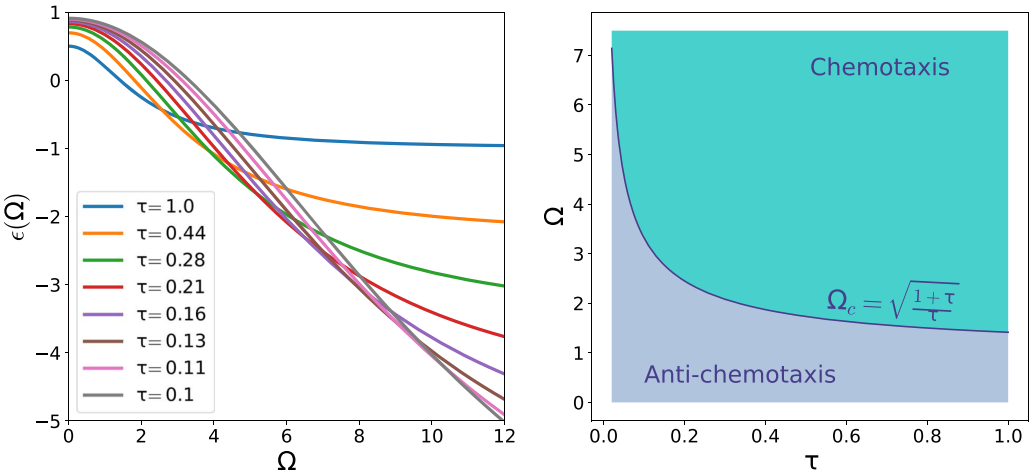

FIG. 4. Left: ϵ as a function of Ω for different values of τ. For vanishing torque, the parameter $\epsilon \to \frac{1}{1+\tau}$, whereas for large torque $\epsilon \to -\frac{1}{\tau}$. With increasing active torque, a dimer switches behavior from antichemotactic $(\epsilon > 0)$ to chemotactic $\epsilon < 0$. Right: Phase diagram in (Ω, τ) plane. The blue critical curve separates the chemotactic from the anti-chemotactic region. In particular, for small spring relaxation time, it is much harder for the dimer to switch its tactic behavior as the threshold torque tends to diverge.

Published under an exclusive license by AIP Publishing

III. ODD DIFFUSION

In Sec. II, we demonstrated how two interacting self-propelled particles driven by microscopic opposite torques can exhibit, for sufficiently high torques, chemotactic behavior. The single components of this molecule belong to a class of systems defined as odd diffusive. This kind of system, usually characterized by a break in time reversal and parity symmetry, has antisymmetric components in the diffusion tensor and flows perpendicular to the density gradient. Recently, the analysis of odd diffusive systems has attracted a lot of attention for both equilibrium and out-of-equilibrium systems such as passive/active charged particles in a magnetic field, see e.g., Refs. 30–33. In the case of charged self-propelled (active) particles immersed in a magnetic field, rather than a microscopic driving torque, it is the Lorentz force that induces a certain chirality. Despite the different physical origins underlying their odd diffusive behavior, both self-propelled particles (with torque induced chirality and Lorentz force induced chirality) are characterized by very similar dynamics. This similarity can be better appreciated from a comparison of their coarse-grained FPEs (derived in Secs. S2 and S3 of the supplementary material), where one integrates out the rotational degree of freedom. In particular, for a single ACP with spatially homogeneous driving torque ω and an activity function v_C in $d = 2$, we have

$$\partial_t \rho(\boldsymbol{r},t) = \nabla_{\boldsymbol{r}} \cdot \left[\left(\frac{v_C^2}{2D_R} \underline{\underline{M}}^{-1} + D_T \mathbf{1} \right) \nabla_{\boldsymbol{r}} \rho(\boldsymbol{r},t) \right], \tag{10}$$

with $\underline{\underline{M}} = \mathbf{1} + \frac{\omega}{D_R}\boldsymbol{\varepsilon}$ and $\boldsymbol{\varepsilon}$ the totally antisymmetric Levi-Cività tensor in two dimensions. For a charged self-propelled particle immersed in homogeneous magnetic field B and activity v_B, we have instead

$$\partial_t \rho(\boldsymbol{r},t) = \nabla \cdot \left[\left(\frac{v_B^2}{2D_R} \frac{1}{1+\kappa^2} \mathbf{1} + D_T \underline{\underline{\Gamma}}^{-1} \right) \nabla \rho(\boldsymbol{r},t) \right], \tag{11}$$

with $\gamma \underline{\underline{\Gamma}} = \gamma(\mathbf{1} - \kappa\boldsymbol{\varepsilon})$ the effective rank-2 friction tensor and $\kappa = \frac{qB}{\gamma}$. The two equations present a similar structure, with both diffusion tensors (expressions in round brackets) containing an antisymmetric component. They can even be equivalent if the following relationships hold:

$$\begin{cases} v_C^2 = -2D_T \dfrac{D_R^2 + \omega^2}{1+\kappa^2} \dfrac{\kappa}{\omega}, \\ v_B^2 = 2D_R D_T \kappa \left(\kappa - \dfrac{D_R}{\omega} \right). \end{cases} \tag{12}$$

Given this intriguing similarity between the two systems, it is natural to wonder whether this extends to their chemotactic behavior. In particular, can two self-propelled oppositely charged interacting particles immersed in a magnetic field $\boldsymbol{B} = B\hat{\boldsymbol{z}}$ cooperate in such a way as to exhibit chemotaxis, similarly to what has been demonstrated for a dimer composed of two active particles driven by opposite microscopic torques?

We show below that, despite the suggestive similarity to active chiral dimers, such charged dimers are always antichemotactic. To prove that, we need to work out an expression for the steady state density of the charged dimer. The derivation is similar to the one outlined in Sec. II for a dimer composed of active particles driven by a torque (for details, see Sec. S4 of the supplementary material) and starts from the evolution of the joint probability density,

$$\partial_t P(\boldsymbol{r}_1, \boldsymbol{r}_2, \theta_1, \theta_2, t) = \left(\hat{\mathcal{L}}_1 + \hat{\mathcal{L}}_2 + \hat{\mathcal{L}}_{rot} \right) P \tag{13}$$

with

$$\begin{aligned} \hat{\mathcal{L}}_1 &= \nabla_{\boldsymbol{r}_1} \cdot \left[-\underline{\underline{\Gamma}}_+^{-1} \left(\frac{1}{\gamma} \boldsymbol{F} + v_a(\boldsymbol{r}_1) \boldsymbol{p}_1 + D_T \nabla_{\boldsymbol{r}_1} \right) \right], \\ \hat{\mathcal{L}}_2 &= \nabla_{\boldsymbol{r}_2} \cdot \left[-\underline{\underline{\Gamma}}_-^{-1} \left(-\frac{1}{\gamma} \boldsymbol{F} + v_a(\boldsymbol{r}_2) \boldsymbol{p}_2 + D_T \nabla_{\boldsymbol{r}_2} \right) \right], \\ \hat{\mathcal{L}}_{rot} &= D_R \left(\frac{\partial^2}{\partial \theta_1^2} + \frac{\partial^2}{\partial \theta_2^2} \right). \end{aligned} \tag{14}$$

The tensor $\underline{\underline{\Gamma}}_{\pm}$ has the same definition as $\underline{\underline{\Gamma}}$, with the additional subscript denoting the sign of the charge $\pm q$, $\boldsymbol{F}$ is the force experienced by the two monomers due to their attractive interaction, and $v_a(\boldsymbol{r})$ is the activity function. Rewriting (13) in terms of center-of-friction $\boldsymbol{R} = \frac{1}{2}(\underline{\underline{\Gamma}}_+ \boldsymbol{r}_1 + \underline{\underline{\Gamma}}_- \boldsymbol{r}_2)$ and inner coordinate $\boldsymbol{r} = \boldsymbol{r}_1 - \boldsymbol{r}_2$, and following similar steps to the ones presented for an active chiral molecule driven by opposite torques, we get a coarse-grained FPE analogous to (6) with the following drift and diffusion terms:

$$\begin{aligned} D(\boldsymbol{R}) &= \frac{v_a^2(\boldsymbol{R})}{4D_R} + \frac{D_T}{2}, \\ \boldsymbol{V}(\boldsymbol{R}) &= -\frac{1}{2} \epsilon \nabla_R D(\boldsymbol{R}). \end{aligned} \tag{15}$$

The exponent ϵ is defined as

$$\epsilon = \left[1 - \frac{1-\kappa^2}{1+\kappa^2} \left(1 - \frac{1}{1+\tau(1+\kappa^2)} \right) \right], \tag{16}$$

and $\kappa = qB/\gamma$. By imposing again zero flux at steady state, the following density profile can be easily derived:

$$\rho(\boldsymbol{R}) \propto \left[1 + \frac{1}{D_T} \frac{v_a^2(\boldsymbol{R})}{2D_R} \right]^{-\frac{\epsilon}{2}}. \tag{17}$$

We note that the expressions (8) and (17) are equivalent when both the magnetic field B and the torque ω are zero. Indeed, in this case both systems reduce to a dimer of simple active Brownian particles (ABPs). However, for generic non-zero values of B and ω, there is a striking difference between the two systems to be noticed. In the dimer of ACPs, it is possible to change the sign of ϵ by varying the value of the torque ω. This allows the system to explore both a chemotactic and an anti-chemotactic phase. Conversely, for the active dimer immersed in a magnetic field, the value of ϵ is strictly positive regardless of the intensity of B. This constraint prevents the system from exhibiting a chemotactic phase.

IV. DISCUSSION

An active chiral particle preferentially accumulates in low activity regions. However, when two such particles are connected to each other with opposite chiralities, the resulting dimer can become chemotactic with increasing active torque. Such an assembly of active chiral particles might be possible using advanced fabrication

Published under an exclusive license by AIP Publishing

techniques that have been used to assemble colloidal particles into desired structures.[48–53] However, at the colloidal scale, it might be challenging to fabricate such dimers without affecting the rotation of the individual chiral particles.

At the millimeter scale, our predictions could be tested in vibrots that are miniature robots that convert vibrations into rotational and translational motion.[54–57] Vibrots with chiral leg configurations can rotate in both senses and hence mimic active chiral particles of opposite polarities.[58] They can be connected to each other without affecting their rotation.[59] Activity gradients could be realized in a vibrating plate via surface patterning, which modifies the effective friction experienced by a vibrot.

Active chiral particles belong to a class of systems referred to as odd-diffusive. In these systems, probability fluxes are not only along the density gradients but also perpendicular to them.[29,60,61] Odd-diffusive behavior is encoded in the diffusion tensor that has an antisymmetric part [Eqs. (10) and (11)]. We showed that despite sharing the property of odd-diffusion, the two systems, namely, active chiral particles and Brownian particles under Lorentz force, exhibit distinct dynamics such that one cannot be mapped to another in general. We showed this explicitly in the context of the tactic behavior of dimers. Another example concerns the dynamics of charged Rouse dimers under a magnetic field. These dimers exhibit strongly enhanced dynamics, even superballistic behavior, when subjected to a uniform magnetic field.[61] The enhancement of dynamics predicted in charged Rouse dimers under a magnetic field[61] cannot be reproduced by dimers of active chiral particles. An example where the mapping is valid concerns the enhancement of self-diffusion due to interactions in odd-diffusive systems.[60] This theoretical prediction can indeed be tested experimentally using active chiral particles.

Since we considered particles with opposite chiralities, the dimer itself does not show odd-diffusive behavior. This is evident in the scalar valued diffusion coefficient in Eq. (6). Additional work is needed to characterize a dimer with arbitrary chiralities, which will, in general, exhibit odd-diffusive behavior.

SUPPLEMENTARY MATERIAL

See the supplementary material for a detailed derivation of the results presented above.

AUTHOR DECLARATIONS

Conflict of Interest

The authors have no conflicts to disclose.

Author Contributions

Pietro Luigi Muzzeddu: Conceptualization (equal); Data curation (lead); Formal analysis (lead); Writing – original draft (equal). **Hidde Derk Vuijk**: Conceptualization (equal); Writing – original draft (supporting). **Hartmut Löwen**: Conceptualization (equal); Writing – review & editing (supporting). **Jens-Uwe Sommer**: Conceptualization (equal); Writing – review & editing (supporting). **Abhinav Sharma**: Conceptualization (equal); Supervision (lead); Writing – original draft (equal); Writing – review & editing (lead).

DATA AVAILABILITY

The data that support the findings of this study are available within the article and its supplementary material.

REFERENCES

[1]T. Ahamed, A. C. Costa, and G. J. Stephens, "Capturing the continuous complexity of behavior in *Caenorhabditis elegans*," Nat. Phys. **17**, 275–283 (2021).
[2]A. C. Costa, T. Ahamed, and G. J. Stephens, "Adaptive, locally linear models of complex dynamics," Proc. Natl. Acad. Sci. **116**, 1501–1510 (2019).
[3]G. H. Wadhams and J. P. Armitage, "Making sense of it all: Bacterial chemotaxis," Nat. Rev. Mol. Cell Biol. **5**, 1024–1037 (2004).
[4]Y. Tu, "Quantitative modeling of bacterial chemotaxis: Signal amplification and accurate adaptation," Annu. Rev. Biophys. **42**, 337–359 (2013).
[5]S. Sengupta, C. A. Parent, and J. E. Bear, "The principles of directed cell migration," Nat. Rev. Mol. Cell Biol. **22**, 529–547 (2021).
[6]H. C. Berg, *E. Coli in Motion* (Springer Science and Business Media, 2008).
[7]M. E. Cates, "Diffusive transport without detailed balance in motile bacteria: Does microbiology need statistical physics?," Rep. Prog. Phys. **75**, 042601 (2012).
[8]J. R. Howse, R. A. L. Jones, A. J. Ryan, T. Gough, R. Vafabakhsh, and R. Golestanian, "Self-Motile colloidal particles: From directed propulsion to random walk," Phys. Rev. Lett. **99**, 048102 (2007).
[9]W. Gao, A. Pei, R. Dong, and J. Wang, "Catalytic iridium-based Janus micromotors powered by ultralow levels of chemical fuels," J. Am. Chem. Soc. **136**, 2276–2279 (2014).
[10]A. Y. Jee, Y. K. Cho, S. Granick, and T. Tlusty, "Catalytic enzymes are active matter," Proc. Natl. Acad. Sci. **115**, E10812–E10821 (2018).
[11]J. Stenhammar, R. Wittkowski, D. Marenduzzo, and M. E. Cates, "Light-induced self-assembly of active rectification devices," Sci. Adv. **2**, e1501850 (2016).
[12]L. Caprini, U. Marini Bettolo Marconi, R. Wittmann, and H. Löwen, "Dynamics of active particles with space-dependent swim velocity," Soft Matter **18**, 1412–1422 (2022).
[13]G. S. Fraenkel and D. L. Gunn, *The Orientation of Animals: Kineses Taxes and Compass Reactions, Dover Books on Biology and Medicine* (Dover Publications, New York, 1961).
[14]M. J. Schnitzer, "Theory of continuum random walks and application to chemotaxis," Phys. Rev. E **48**, 2553 (1993).
[15]A. Sharma and J. M. Brader, "Brownian systems with spatially inhomogeneous activity," Phys. Rev. E **96**, 032604 (2017).
[16]T. Mano, J. B. Delfau, J. Iwasawa, and M. Sano, "Optimal run-and-tumble–based transportation of a Janus particle with active steering," Proc. Natl. Acad. Sci. **114**, E2580–E2589 (2017).
[17]B. Qian, D. Montiel, A. Bregulla, F. Cichos, and H. Yang, "Harnessing thermal fluctuations for purposeful activities: The manipulation of single micro-swimmers by adaptive photon nudging," Chem. Sci. **4**, 1420–1429 (2013).
[18]H. Massana-Cid, C. Maggi, G. Frangipane, and R. Di Leonardo, "Rectification and confinement of photokinetic bacteria in an optical feedback loop," Nat. Commun. **13**, 2740 (2022).
[19]H. D. Vuijk, H. Merlitz, M. Lang, A. Sharma, and J.-U. Sommer, "Chemotaxis of cargo-carrying self-propelled particles," Phys. Rev. Lett. **126**, 208102 (2021).
[20]R. G. Winkler, J. Elgeti, and G. Gompper, "Active polymers—Emergent conformational and dynamical properties: A brief review," J. Phys. Soc. Jpn. **86**, 101014 (2017).
[21]S. M. Mousavi, G. Gompper, and R. G. Winkler, "Active Brownian ring polymers," J. Chem. Phys. **150**, 064913 (2019).
[22]R. G. Winkler and G. Gompper, "The physics of active polymers and filaments," J. Chem. Phys. **153**, 040901 (2020).

Published under an exclusive license by AIP Publishing

[23]A. Martín-Gómez, T. Eisenstecken, G. Gompper, and R. G. Winkler, "Active Brownian filaments with hydrodynamic interactions: Conformations and dynamics," Soft Matter **15**, 3957–3969 (2019).
[24]T. Eisenstecken and R. G. Winkler, "Path integral description of semiflexible active Brownian polymers," J. Chem. Phys. **156**, 064105 (2022).
[25]A. Kaiser, S. Babel, B. ten Hagen, C. von Ferber, and H. Löwen, "How does a flexible chain of active particles swell?," J. Chem. Phys. **142**, 124905 (2015).
[26]S. Ebbens, R. A. Jones, A. J. Ryan, R. Golestanian, and J. R. Howse, "Self-assembled autonomous runners and tumblers," Phys. Rev. E **82**, 015304 (2010).
[27]H. Löwen, "Active colloidal molecules," EPL **121**, 58001 (2018).
[28]H. D. Vuijk, S. Klemphan, H. Merlitz, J.-U. Sommer, and A. Sharma, "Active colloidal molecules in activity gradients," Phys. Rev. E **106**, 014617 (2022).
[29]C. Hargus, J. M. Epstein, and K. K. Mandadapu, "Odd diffusivity of chiral random motion," Phys. Rev. Lett. **127**, 178001 (2021).
[30]H. D. Vuijk, J. U. Sommer, H. Merlitz, J. M. Brader, and A. Sharma, "Lorentz forces induce inhomogeneity and flux in active systems," Phys. Rev. Res. **2**, 013320 (2020).
[31]I. Abdoli, H. D. Vuijk, J. U. Sommer, J. M. Brader, and A. Sharma, "Nondiffusive fluxes in Brownian system with Lorentz force," Phys. Rev. E **101**, 012120 (2020).
[32]I. Abdoli, H. D. Vuijk, R. Wittmann, J. U. Sommer, J. M. Brader, and A. Sharma, "Stationary state in Brownian systems with Lorentz force," Phys. Rev. Res. **2**, 023381 (2020).
[33]I. Abdoli, E. Kalz, H. D. Vuijk, R. Wittmann, J.-U. Sommer, J. M. Brader, and A. Sharma, "Correlations in multithermostat Brownian systems with Lorentz force," New J. Phys. **22**, 093057 (2020).
[34]I. Abdoli, R. Wittmann, J. Michael Brader, J.-U. Sommer, H. Löwen, and A. Sharma, "Tunable Brownian magneto heat pump," Sci. Rep. **12**, 13405 (2022).
[35]C. Bechinger, R. Di Leonardo, H. Löwen, C. Reichhardt, G. Volpe, and G. Volpe, "Active particles in complex and crowded environments," Rev. Mod. Phys. **88**, 045006 (2016).
[36]T. F. Farage, P. Krinninger, and J. M. Brader, "Effective interactions in active Brownian suspensions," Phys. Rev. E **91**, 042310 (2015).
[37]L. Caprini and U. Marini Bettolo Marconi, "Active matter at high density: Velocity distribution and kinetic temperature," J. Chem. Phys. **153**, 184901 (2020).
[38]A. Sharma, R. Wittmann, and J. M. Brader, "Escape rate of active particles in the effective equilibrium approach," Phys. Rev. E **95**, 012115 (2017).
[39]R. Golestanian, "Anomalous diffusion of symmetric and asymmetric active colloids," Phys. Rev. Lett. **102**, 188305 (2009).
[40]C. Lozano, B. ten Hagen, H. Löwen, and C. Bechinger, "Phototaxis of synthetic microswimmers in optical landscapes," Nat. Commun. **7**, 12828 (2016).
[41]M. N. Popescu, M. Tasinkevych, and S. Dietrich, "Pulling and pushing a cargo with a catalytically active carrier," EPL **95**, 28004 (2011).
[42]M. N. Popescu, W. E. Uspal, Z. Eskandari, M. Tasinkevych, and S. Dietrich, "Effective squirmer models for self-phoretic chemically active spherical colloids," Eur. Phys. J. E **41**, 145 (2018).
[43]S. Y. Reigh and R. Kapral, "Catalytic dimer nanomotors: Continuum theory and microscopic dynamics," Soft Matter **11**, 3149–3158 (2015).
[44]S. Y. Reigh, P. Chuphal, S. Thakur, and R. Kapral, "Diffusiophoretically induced interactions between chemically active and inert particles," Soft Matter **14**, 6043–6057 (2018).
[45]J. A. Kromer, N. de la Cruz, and B. M. Friedrich, "Chemokinetic scattering, trapping, and avoidance of active Brownian particles," Phys. Rev. Lett. **124**, 118101 (2020); arXiv:1904.11020.
[46]C. Lozano and C. Bechinger, "Diffusing wave paradox of phototactic particles in traveling light pulses," Nat. Commun. **10**, 2495 (2019).
[47]S. Jahanshahi, C. Lozano, B. Liebchen, H. Löwen, and C. Bechinger, "Realization of a motility-trap for active particles," Commun. Phys. **3**, 127 (2020).
[48]Q. Chen, S. C. Bae, and S. Granick, "Directed self-assembly of a colloidal Kagome lattice," Nature **469**, 381–384 (2011).
[49]E. Bianchi, R. Blaak, and C. N. Likos, "Patchy colloids: State of the art and perspectives," Phys. Chem. Chem. Phys. **13**, 6397 (2011).
[50]S. Sacanna, W. T. M. Irvine, P. M. Chaikin, and D. J. Pine, "Lock and key colloids," Nature **464**, 575–578 (2010).
[51]S. C. Glotzer and M. J. Solomon, "Anisotropy of building blocks and their assembly into complex structures," Nat. Mater. **6**, 557–562 (2007).
[52]J. Zhang, J. Yan, and S. Granick, "Directed self-assembly pathways of active colloidal clusters," Angew. Chem. **128**, 5252–5255 (2016).
[53]M. N. Popescu, "Chemically active particles: From one to few on the way to many," Langmuir **36**, 6861–6870 (2020).
[54]E. Altshuler, J. M. Pastor, A. Garcimartín, I. Zuriguel, and D. Maza, "*Vibrot*, a simple device for the conversion of vibration into rotation mediated by friction: Preliminary evaluation," PLoS One **8**, e67838 (2013).
[55]C. Scholz, S. D'Silva, and T. Pöschel, "Ratcheting and tumbling motion of Vibrots," New J. Phys. **18**, 123001 (2016).
[56]C. Scholz and T. Pöschel, "Velocity distribution of a homogeneously driven two-dimensional granular gas," Phys. Rev. Lett. **118**, 198003 (2017).
[57]M. Broseghini, C. Ceccolini, C. Della Volpe, and S. Siboni, "The Notched Stick, an ancient vibrot example," PLoS One **14**, e0218666 (2019).
[58]C. Scholz, M. Engel, and T. Pöschel, "Rotating robots move collectively and self-organize," Nat. Commun. **9**, 931–938 (2018).
[59]C. Scholz, A. Ldov, T. Pöschel, M. Engel, and H. Löwen, "Surfactants and rotelles in active chiral fluids," Sci. Adv. **7**, eabf8998 (2021).
[60]E. Kalz, H. D. Vuijk, I. Abdoli, J. U. Sommer, H. Löwen, and A. Sharma, "Collisions enhance self-diffusion in odd-diffusive systems," Phys. Rev. Lett. **129**, 090601 (2022).
[61]R. Shinde, J. U. Sommer, H. Löwen, and A. Sharma, "Strongly enhanced dynamics of a charged Rouse dimer by an external magnetic field," PNAS Nexus **1**, pgac119 (2022).

Published under an exclusive license by AIP Publishing